

## COSMIC EMULATION: THE CONCENTRATION-MASS RELATION FOR $\Lambda$ CDM UNIVERSES

JULIANA KWAN<sup>1</sup>, SUMAN BHATTACHARYA<sup>1,2</sup>, KATRIN HEITMANN<sup>1,2,3,4</sup>, AND SALMAN HABIB<sup>1,2,3,4</sup>

<sup>1</sup> High Energy Physics Division, Argonne National Laboratory, Lemont, IL 60439

<sup>2</sup> Kavli Institute for Cosmological Physics, The University of Chicago, Chicago, IL 60637

<sup>3</sup> Mathematics and Computer Science Division, Argonne National Laboratory, Lemont, IL 60439

<sup>4</sup> Computation Institute, The University of Chicago, Chicago, IL 60637

*Draft version September 12, 2021*

### ABSTRACT

The concentration-mass relation for dark matter-dominated halos is one of the essential results expected from a theory of structure formation. We present a simple prediction scheme, a *cosmic emulator*, for the  $c-M$  relation as a function of cosmological parameters for  $w$ CDM models. The emulator is constructed from 37 individual models, with three nested  $N$ -body gravity-only simulations carried out for each model. The mass range covered by the emulator is  $2 \cdot 10^{12} M_{\odot} < M < 10^{15} M_{\odot}$  with a corresponding redshift range of  $z = 0 - 1$ . Over this range of mass and redshift, as well as the variation of cosmological parameters studied, the mean halo concentration varies from  $c \sim 2$  to  $c \sim 8$ . The distribution of the concentration at fixed mass is Gaussian with a standard deviation of one-third of the mean value, almost independent of cosmology, mass, and redshift over the ranges probed by the simulations. We compare results from the emulator with previously derived heuristic analytic fits for the  $c-M$  relation, finding that they underestimate the halo concentration at high masses. Using the emulator to investigate the cosmology dependence of the  $c-M$  relation over the currently allowable range of values, we find – not surprisingly – that  $\sigma_8$  and  $\omega_m$  influence it considerably, but also that the dark energy equation of state parameter  $w$  has a substantial effect. In general, the concentration of lower-mass halos is more sensitive to changes in cosmological parameters as compared to cluster mass halos.

The  $c-M$  emulator is publicly available from <http://www.hep.anl.gov/cosmology/CosmicEmu>.

*Subject headings:* methods: statistical — cosmology: large-scale structure of the universe

### 1. INTRODUCTION

Over the last three decades, cosmology has made tremendous progress, culminating in the so-called “Standard Model of Cosmology”. The two main components of the Standard Model are a mysterious dark energy, leading to a late-time accelerated expansion, and a dark matter component making up roughly 25% of the total matter-energy budget of the Universe. The evolution of structure in the Universe from the earliest accessible times to today is successfully described by a theory based on the gravitational instability – the distribution of galaxies in the Universe, for example, is remarkably well reproduced by this paradigm. Clusters and groups of galaxies are major building blocks of the large-scale structure and measurements of their abundance provide a powerful cosmological probe. Large, gravity-only  $N$ -body simulations have been remarkably successful in providing a consistent picture of the formation of the large-scale structure from the very early, small Gaussian density fluctuations to the halos, voids, and filaments we observe today.

A surprising discovery from these simulations (Navarro et al. 1996, 1997) was that the dark matter-dominated halos – over a wide mass range typical of dwarf galaxies to massive clusters – share a basically universal density profile. In detail, it was shown that the spherically averaged density profile of relaxed halos formed in simulations can be described by what is now commonly known as the NFW (Navarro-Frenk-White) profile. The NFW profile is described by two parameters, the normalization and the characteristic scale radius of the halo or equivalently its (dimensionless) concentration.

Aside from the distribution of halo masses, halo profiles are also of considerable interest. The profiles can be measured directly for individual massive halos by a variety of observational methods, or inferred indirectly for less massive halos using statistical lensing probes. Halo profiles are also a key input in

halo occupation distribution (HOD) modeling of the distribution of galaxies. NFW profiles (or minor variants thereof) are consistent with current observations (Bhattacharya et al. 2011) and, as the observations continue to improve, a corresponding improvement in theoretical predictions for (NFW) halo concentrations as a function of cosmological parameters is needed. As scatter in the  $c-M$  relation is considerable, in principle, this would encompass knowing the actual distribution of halo concentrations as a function of halo mass.

Quantitative predictions for the  $c-M$  relation from a first principles analytic approach are difficult to obtain, due to the highly nonlinear dynamics involved in the formation of halos. Accurate predictions can only be obtained from computationally expensive, high-resolution simulations. These simulations need to cover large volumes in order to yield good statistics, especially in the cluster mass regime, as well as high force resolution to reliably resolve the halo profiles. In recent years, the focus has therefore been on generating predictions for one cosmology around the best-fit WMAP (Wilkinson Microwave Anisotropy Probe) results of that time (e.g., Duffy et al. 2008, Bhattacharya et al. 2011, Prada et al. 2012). The fitting functions so generated cannot be extended beyond the cosmological model they have been tuned for. Heuristic models that aim to extend this reach, e.g. those by Bullock et al. (2001) and Eke et al. (2001) and improvements thereof (Macciò et al. 2008) do not lead to the desired accuracy, as discussed in Duffy et al. (2008). Other discussions of this issue can be found in Gao et al. (2008), Hayashi & White (2008), and Zhao et al. (2009).

In order to overcome the many shortcomings of fitting functions as a general approach in cosmology, we have recently developed the “Cosmic Calibration Framework” (CCF) to provide accurate prediction schemes for cosmological observables (Heitmann et al. 2006; Habib et al. 2007). The aim of the CCF is to build

codes that act as very fast – basically instantaneous – prediction tools for large scale structure observables such as the nonlinear power spectrum (Heitmann et al. 2010, 2009; Lawrence et al. 2010), mass functions for different halo definitions, or the concentration-mass relation – as discussed here. Predicting these observables requires running a number of high-performance simulations to reliably resolve the nonlinear regime of structure formation. The CCF provides a powerful way to build precision prediction tools from a limited number of computationally expensive simulations.

At the heart of the CCF lies a sophisticated sampling scheme that provides an optimal sampling strategy for the cosmological models to be simulated (we use orthogonal array-based Latin hypercube as well as symmetric Latin hypercube designs; an introduction to the general sampling strategy is provided in Santner et al. 2003), an optimal representation to translate the measurements from the simulations into functions that can be easily interpolated (a principal component basis turns out to be an efficient representation), and finally a very accurate interpolation scheme (our choice here is Gaussian process modeling).

The CCF was first introduced in Heitmann et al. (2006) and a more detailed description and examples are provided in Habib et al. (2007). In a series of three papers (Coyote Universe I-III) we developed an emulator for the matter power spectrum for a five dimensional parameter space covering  $\theta = \{\omega_b, \omega_m, n_s, w, \sigma_8\}$ . This emulator provides predictions for the power spectrum for  $w$ CDM cosmologies out to  $k \sim 1 \text{ Mpc}^{-1}$  at the 1% accuracy level for a redshift range of  $0 \leq z \leq 1$ . In Schneider et al. (2008) the work was extended to derive an approximate statistical model for the sample variance distribution of the nonlinear matter power spectrum. Eifler (2012) used the emulator to generate a weak lensing prediction code to calculate various second-order cosmic shear statistics, e.g., shear power spectrum, shear-shear correlation function, ring statistics and Complete Orthogonal Set of EB-mode Integrals (COSEBIs).

The focus of this paper is the development of an emulator for the concentration-mass relation for  $w$ CDM cosmologies. We use the same base set of simulations as in Lawrence et al. (2010), consisting of 37 cosmological models and a single 1300 Mpc volume, high-resolution simulation for each model. This simulation set is augmented here with a set of new, higher resolution simulations. These simulations cover smaller volumes (a 360 Mpc and a 180 Mpc simulation for each model) to obtain good statistics over a large range of halo masses. For each model we measure the best-fit concentration-mass ( $c-M$ ) relation, assuming a simple power law form. The fits lay the foundation for building the emulator that provides predictions for the  $c-M$  relation within the  $w$ CDM parameter space covered by the original simulations. In redshift, the emulator covers the range between  $z = 0$  and  $z = 1$ . We provide a fast code that delivers the mean  $c-M$  relations for  $w$ CDM cosmologies to good accuracy<sup>1</sup>.

As is well-known, the  $c-M$  relation has considerable scatter and, in principle, it is not obvious that this scatter should have a simple form, and what its cosmological dependence might be. However, as discussed in Bhattacharya et al. (2011), the scatter has a simple Gaussian form in  $w$ CDM models, and moreover, even though the mean  $c-M$  relation is clearly cosmology-dependent, as is the associated concentration variance,  $\sigma_c^2(M)$ , the ratio of  $\sigma_c(M)$  to the mean concentration is close to  $1/3$ ,

independent of cosmology, mass, or redshift. This means that once an emulator for the  $c-M$  relation is in hand, the concentration standard deviation is given automatically by a simple relation.

The paper is organized as follows. After a brief outline of the halo concentration measurements from the simulations, we describe the cosmological model space and the simulation suite used to build the emulator. In Section 3 we also discuss the generation of the smooth prediction for the concentration-mass relation for each model that underlies the interpolation scheme for building the emulator. We give a brief description on how to build the emulator in Section 4 and show some examples from the working emulator and test results verifying its accuracy. We also compare our results to currently used fitting formulae and investigate the cosmology dependence of the  $c-M$  relation in some detail. Finally, we provide a conclusion and outlook in Section 5.

## 2. CONCENTRATION-MASS RELATION

We study the concentration-mass relation in the regime of bright galaxies to clusters of galaxies, spanning halo mass ranges between  $2 \cdot 10^{12} M_\odot$  to  $10^{15} M_\odot$ , while varying  $w$ CDM cosmological parameters. A detailed description on how to measure halo concentrations from simulations and a discussion of possible systematics is given in Bhattacharya et al. (2011). We follow the same approach in this paper and give here a brief summary of the main steps in measuring the  $c-M$  relation in our simulations.

As a first step, we identify halos using a fast parallel friends-of-friends (FOF) finder (Woodring et al. 2011) with linking length  $b = 0.2$ . Once a halo is found, we define its center via a density maximum criteria – the location of the particle with the maximum number of neighbors. This definition of the halo center is very close to that given by the halo’s potential minimum. Given a halo center, we grow spheres around it and compute the mass in radial bins. Note that even though an FOF finder is used, the actual halo mass is defined by a spherical overdensity method, consistent with what is done in observations. (For discussions on halo mass, see, e.g., White 2001, Lukić et al. 2009, and More et al. 2011). The NFW form for the spherically averaged halo profile is a function of two parameters, one of which is constrained by the halo mass. Here we fit the mass profile using both total halo mass and concentration as free variables. Although the mass could be measured independently of the concentration, the joint analysis is potentially less sensitive to fitting bias.

We write the NFW profile as

$$\rho(r) = \frac{\delta \rho_{\text{crit}}}{(r/r_s)(1+r/r_s)^2}, \quad (1)$$

where  $\delta$  is a characteristic dimensionless density, and  $r_s$  is the scale radius of the NFW profile. The concentration of a halo is defined as  $c_\Delta = r_\Delta/r_s$ , where  $\Delta$  is the overdensity with respect to the *critical density* of the Universe,  $\rho_{\text{crit}} = 3H^2/8\pi G$ , and  $r_\Delta$  is the radius at which the enclosed mass,  $M_\Delta$ , equals the volume of the sphere times the density  $\Delta\rho_{\text{crit}}$ . We compute concentrations corresponding to  $\Delta = 200$ , corresponding in turn to  $c_{200} = R_{200}/r_s$ .

The mass enclosed within a radius  $r$  for an NFW halo is given by

$$M(< r) = m(c_\Delta r/R_{200})/m(c_{200})M_{200}, \quad (2)$$

where  $m(y) = \ln(1+y) - y/(1+y)$ . The mass in a radial bin is

<sup>1</sup> <http://www.hep.anl.gov/cosmology/CosmicEmu>

TABLE 1

THE PARAMETERS FOR THE 37+1 MODELS WHICH DEFINE THE SAMPLE SPACE. SEE TEXT FOR FURTHER DETAILS.													
#	$\omega_m$	$\omega_b$	$n_s$	$-w$	$\sigma_8$	$h$	#	$\omega_m$	$\omega_b$	$n_s$	$-w$	$\sigma_8$	$h$
M000	0.1296	0.0224	0.9700	1.000	0.8000	0.7200	M019	0.1279	0.0232	0.8629	1.184	0.6159	0.8120
M001	0.1539	0.0231	0.9468	0.816	0.8161	0.5977	M020	0.1290	0.0220	1.0242	0.797	0.7972	0.6442
M002	0.1460	0.0227	0.8952	0.758	0.8548	0.5970	M021	0.1335	0.0221	1.0371	1.165	0.6563	0.7601
M003	0.1324	0.0235	0.9984	0.874	0.8484	0.6763	M022	0.1505	0.0225	1.0500	1.107	0.7678	0.6736
M004	0.1381	0.0227	0.9339	1.087	0.7000	0.7204	M023	0.1211	0.0220	0.9016	1.261	0.6664	0.8694
M005	0.1358	0.0216	0.9726	1.242	0.8226	0.7669	M024	0.1302	0.0226	0.9532	1.300	0.6644	0.8380
M006	0.1516	0.0229	0.9145	1.223	0.6705	0.7040	M025	0.1494	0.0217	1.0113	0.719	0.7398	0.5724
M007	0.1268	0.0223	0.9210	0.700	0.7474	0.6189	M026	0.1347	0.0232	0.9081	0.952	0.7995	0.6931
M008	0.1448	0.0223	0.9855	1.203	0.8090	0.7218	M027	0.1369	0.0224	0.8500	0.836	0.7111	0.6387
M009	0.1392	0.0234	0.9790	0.739	0.6692	0.6127	M028	0.1527	0.0222	0.8694	0.932	0.8068	0.6189
M010	0.1403	0.0218	0.8565	0.990	0.7556	0.6695	M029	0.1256	0.0228	1.0435	0.913	0.7087	0.7067
M011	0.1437	0.0234	0.8823	1.126	0.7276	0.7177	M030	0.1234	0.0230	0.8758	0.777	0.6739	0.6626
M012	0.1223	0.0225	1.0048	0.971	0.6271	0.7396	M031	0.1550	0.0219	0.9919	1.068	0.7041	0.6394
M013	0.1482	0.0221	0.9597	0.855	0.6508	0.6107	M032	0.1200	0.0229	0.9661	1.048	0.7556	0.7901
M014	0.1471	0.0233	1.0306	1.010	0.7075	0.6688	M033	0.1399	0.0225	1.0407	1.147	0.8645	0.7286
M015	0.1415	0.0230	1.0177	1.281	0.7692	0.7737	M034	0.1497	0.0227	0.9239	1.000	0.8734	0.6510
M016	0.1245	0.0218	0.9403	1.145	0.7437	0.7929	M035	0.1485	0.0221	0.9604	0.853	0.8822	0.6100
M017	0.1426	0.0215	0.9274	0.893	0.6865	0.6305	M036	0.1216	0.0233	0.9387	0.706	0.8911	0.6421
M018	0.1313	0.0216	0.8887	1.029	0.6440	0.7136	M037	0.1495	0.0228	1.0233	1.294	0.9000	0.7313

then

$$M_i = M(< r_i) - M(< r_{i-1}). \quad (3)$$

We then fit Eq. 3 to the mass contained in the radial bins of each halo, by minimizing the associated value of  $\chi^2$  as

$$\chi^2 = \sum_i \frac{(M_i^{sim} - M_i)^2}{(M_i^{sim})^2 / n_i}, \quad (4)$$

where the sum is over the radial bins,  $n_i$  is the number of particles in a radial bin,  $M_i^{sim}$  is the mass in bin  $i$  calculated from the simulations and  $M_i$  is the mass calculated assuming the NFW profile. The advantage of fitting mass in radial bins rather than the density is that the bin center does not have to be specified. Note that we explicitly account for the finite number of particles in a bin. This leads to a slightly larger error in the profile fitting but minimizes any possible bias due to the finite number of particles, especially near the halo center.

We fit for two parameters – the normalization of the profile and the concentration. Halo profiles are fitted in the radial range of approximately  $(0.1 - 1)R_{vir}$ . This choice is motivated partly by the observations of concentrations that typically exclude the central region of clusters (e.g., observations by Oguri et al. 2011). More significantly, however, this excludes the central core which is sensitive to the effects of baryonic physics and numerical errors arising from limitations in both mass and force resolution. Duffy et al. (2010) have shown that, at  $r < 0.1R_{vir}$ , cluster halo profiles are potentially sensitive to the impact of baryons with the profiles being affected at  $r = 0.05R_{vir}$  by as much as a factor of 2.

The  $c - M$  relation is calculated by weighing the individual concentrations by the halo mass,

$$c(M) = \frac{\sum_i c_i M_i}{\sum_i M_i}, \quad (5)$$

where the sum is over the number,  $N_i$ , of the halos in a mass bin. The mass of the bin is given by

$$M = \sum_i M_i / N_i. \quad (6)$$

The error on  $c(M)$  is the mass-weighted error on the individual fits plus the Poisson error due to the finite number of halos in an individual bin added in quadrature,

$$\Delta c(M) = \sqrt{\left( \frac{\sum_i \Delta c_i M_i}{\sum_i M_i} \right)^2 + \frac{c^2(M)}{N_i}}, \quad (7)$$

where  $\Delta c_i$  is the individual concentration error for each halo. The first term dominates towards the lower mass end where the individual halos have smaller number of particles and the second term dominates towards the higher mass end, where there are fewer halos to average over.

### 3. COSMOLOGICAL MODELS AND SIMULATION SETS

We now describe the cosmological model space covered by our prediction scheme and the simulations used to construct it. The emulator is based on 37 cosmological models spanning the class of  $w$ CDM cosmologies. We allow for variations of the following five parameters:

$$\theta = \{\omega_b, \omega_m, n_s, w, \sigma_8\}. \quad (8)$$

The 37 models are chosen to lie within the ranges:

$$\begin{aligned} 0.0215 < \omega_b < 0.0235, \\ 0.120 < \omega_m < 0.155, \\ 0.85 < n_s < 1.05, \\ -1.30 < w < -0.70, \\ 0.616 < \sigma_8 < 0.9, \end{aligned} \quad (9)$$

which are picked based on current constraints from CMB measurements (Komatsu et al. 2011). Following the approach in Lawrence et al. (2010) we lock the value of the Hubble parameter  $h$  to the best-fit value for each model, given the measurement of the distance to the surface of last scattering. The values for  $h$  then range from  $0.55 < h < 0.85$ . In addition to the 37 models, we run one  $\Lambda$ CDM model (M000 in Table 1) which is not used to build the emulator. Instead we use this model as a control for testing the accuracy of the emulator. All 37+1 models are specified in detail in Table 1.

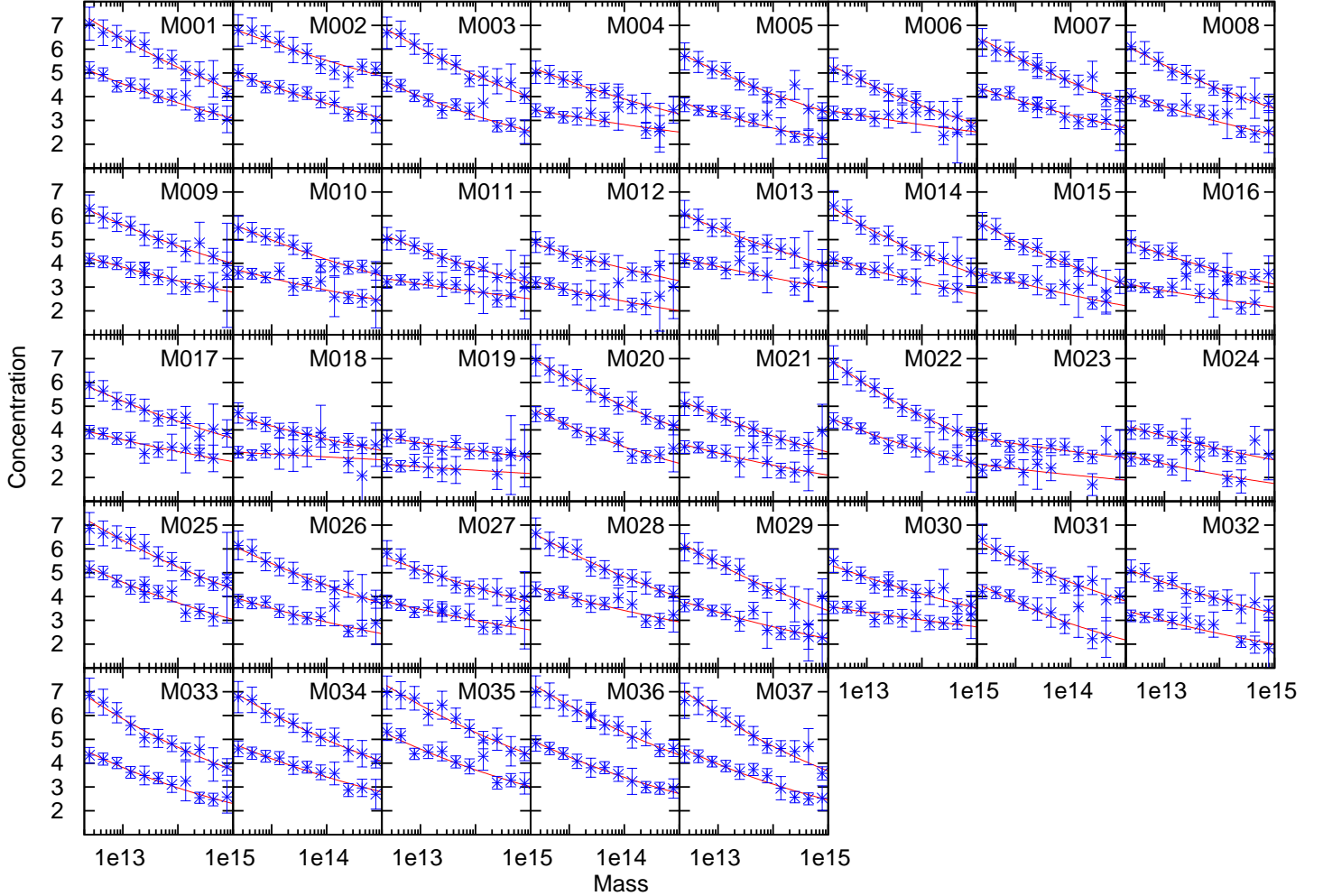


FIG. 1.— Concentration-mass relations for 37  $w$ CDM cosmologies. The blue points show the measurements from the three simulations per model while the red lines show the best-fit power law for each measurement. In each subplot we show the results for  $z = 0$  and  $z = 1$  (upper and lower curve respectively). We find the best-fit power law separately for both redshifts. Models with low values for  $\sigma_8$  in general also exhibit lower  $c-M$  relations (e.g. M012, M018, M019). The fits shown here are the foundation for building the emulator described in Section 4.

The specific model selection process is described at length in Heitmann et al. (2009). In summary, it is based on Symmetric Latin Hypercube (SLH) sampling (Li & Ye 2000); this sampling strategy provides a scheme that guarantees good coverage of the parameter hypercube. In our specific case we choose an SLH design that has good space filling properties in the case of two-dimensional projections in parameter space. In other words, if any two parameters are displayed in a plane, the plane will be well covered by simulation points. Heitmann et al. (2009) provide an extensive discussion regarding optimal design choices and we refer the interested reader to that paper.

The emulator developed here is valid between  $0 < z < 1$

TABLE 2

BOX SIZES, PARTICLE NUMBERS, AND MASS RESOLUTION.

Length [Mpc]	$N_p^3$	Force res. [kpc]	$m_p$ [ $M_\odot$ ]
1300	$1024^3$	50	$5.7 \cdot 10^{11} \omega_m$
365	$512^3$	10	$1.0 \cdot 10^{11} \omega_m$
180	$512^3$	10	$1.2 \cdot 10^{10} \omega_m$

and covers a halo mass range from  $2 \cdot 10^{12} M_\odot$  to  $10^{15} M_\odot$ . We use different box sizes to cover different mass ranges with sufficient statistics. A summary of the different simulation sizes is given in Table 2. All simulations were carried out with the TreePM code GADGET-2 (Springel 2005a). In previous work (Bhattacharya et al. 2011), we have shown that results from GADGET-2 simulations and those with HACC (Habib et al. 2009; Pope et al. 2010) produce completely consistent results. Results from a recent cluster re-simulation campaign (Wu et al. 2012) are also in good agreement with those of Bhattacharya et al. (2011).

One set of simulations is from the original Coyote Universe suite as described in Lawrence et al. (2010). This set of runs evolves  $1024^3$  particles in  $(1300 \text{ Mpc})^3$  volumes. In addition, we run one realization each per model with  $512^3$  particles with a 10 kpc force resolution in a 365 Mpc box and a 180 Mpc box. A summary of the simulation sets including force and mass resolution is given in Table 2.

We combine the simulation results from the three boxes for each model to obtain measurements spanning the desired mass range. While some models (in particular those with high values of  $\sigma_8$ ) have clusters at even higher masses, the statistics beyond  $10^{15} M_\odot$  are insufficient and we exclude those measurements.

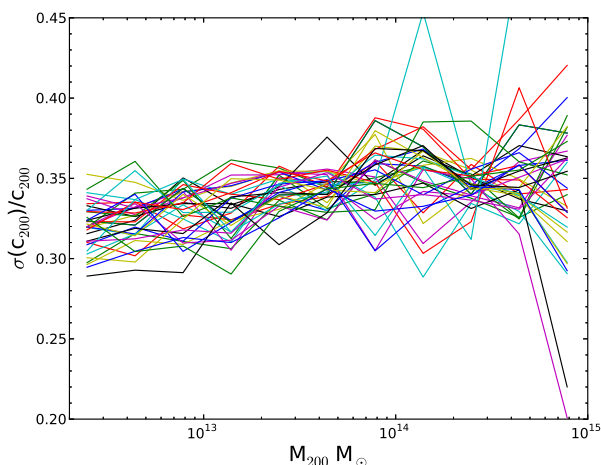


FIG. 2.— Ratio of the standard deviation of the concentration to the mean concentration as a function of mass for all 37 cosmologies at  $z=0$ . While both the standard deviation and the mean concentration are functions of cosmology and redshift, their ratio is essentially invariant, and is approximately  $1/3$ . The distribution of the concentration around the mean is well-fit by a Gaussian distribution (Bhattacharya et al. 2011).

This is also done in order to avoid extrapolations for models where no data points at high masses exist. In order to build an emulator, for each model we have to provide a prediction for the  $c-M$  relation for the same mass range. This ensures that we can provide a consistent set of measurements for the final interpolation process between different models. From the simulation results, we determine for each of the 37+1 cosmologies the best-fit  $c-M$  relation by simply finding the best-fit power law for each model at two redshifts,  $z=0$  and  $z=1$ . The results for the 37 models underlying the emulator are shown in Fig. 1. The blue points show the simulation results while the red curves show the best-fit power law for each model. The upper curves in each plot are obtained at redshift  $z=0$  and the lower curves at  $z=1$ . The concentration values range between  $c \sim 2$  and  $c \sim 8$ . As expected, we find that models with low values of  $\sigma_8$  (e.g., M012, M018, M019 with  $\sigma_8 < 0.65$ ) have depressed  $c-M$  relations. We will return to the cosmology dependence of the  $c-M$  relation in Section 4.2 after constructing the emulator, which will allow us to carry out a comprehensive sensitivity analysis. We reiterate that the fits shown in Fig. 1 are the basis for building the emulator; this procedure is discussed in the next section.

Finally we turn to a discussion of the intrinsic scatter in the  $c-M$  relation. As mentioned earlier, the distribution of concentrations at any given halo mass is Gaussian, and the ratio of  $\sigma_c(M)$  to the mean concentration is an approximate invariant for  $\Lambda$ CDM models, with a value of  $\sim 1/3$  (Bhattacharya et al. 2011), independent of redshift and halo mass. This behavior is exhibited in Fig. 2 where the ratio is computed for all 37 cosmologies as a function of halo mass, at  $z=0$ . Thus, given the  $c-M$  relation from the emulator, the standard deviation at each mass bin can be trivially estimated by multiplying the returned concentration value by  $1/3$ .

#### 4. EMULATOR FOR THE CONCENTRATION-MASS RELATION

##### 4.1. Building the emulator

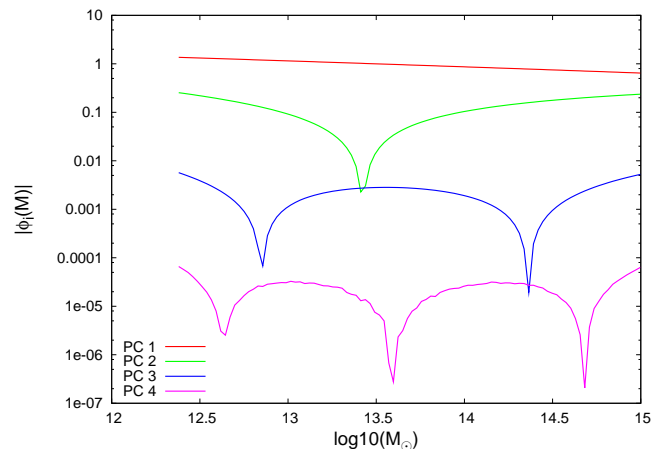


FIG. 3.— First four PC basis vectors,  $\phi_i$ . Absolute values are used to show the dynamic range on a logarithmic scale. Only the first three basis vectors are actually used in the emulation; any others contribute on a scale many orders of magnitude smaller.

In this section, we briefly outline the process for building the  $c-M$  emulator. We follow the procedure explained in Heitmann et al. (2009) and refer the reader to this paper for more complete details. The focus of Heitmann et al. (2009) was on modeling the matter power spectrum rather than the  $c-M$  relation, however, the process is essentially unchanged. Starting with the design of 37 models given in Table 1, we measure the  $c-M$  relation for each cosmology at  $z=0$  and  $z=1$  and fit these with a power law as described in Section 3 to obtain a smooth functional form. First, for every mass bin, the global mean value is subtracted, and then via a simple rescaling, the concentrations are normalized to have unit variance. This produces a zero-mean, unit variance dataset spanning the 37 cosmologies. To reduce the dimensionality of the problem, these normalized functions are then decomposed into principal component (PC) basis functions and only the most significant components are kept. The idea is to apply the interpolation method of choice (Gaussian process modeling in our case) to the coefficients of the basis functions, rather than to the raw data itself (see Heitmann et al. 2009 for details). Figure 3 shows that we only need three PCs to successfully capture the behavior of the  $c-M$  relation since the shape of the relationship remains fairly simple across this set of cosmologies. As explained above, the emulator actually returns the weight on each PC basis function and these can be combined together to give the new  $c-M$  relation. We model the error in the projection to the PC basis with an additional hyperparameter  $\lambda_p$  that can be tuned to represent the level of noise in the data.

A Gaussian process is then used to interpolate between the model results; this means that the  $c-M$  relation for a new cosmology is actually a function drawn from a unit normal distribution. The covariance matrix describes the ‘distance’ between the new model and the set of known models as given by the covariance function. The full covariance matrix,  $\Sigma$ , is composed of one  $\Sigma_l$  for each PC, arranged along the diagonal elements such that:  $\Sigma = \text{diag}(\Sigma_1 \dots \Sigma_n)$  for  $n$  PCs. Each element of  $\Sigma_l$  is given by:

$$\Sigma_{l;ij} = \lambda_l \prod_{k=1}^5 \rho_{kl}^{4(\theta_{ik} - \theta_{jk})^2}, \quad (10)$$

where  $\theta_l$  represents the cosmological parameters and the  $i$  and  $j$  indices run over the number of models spanning the design space (in this case  $i, j = 1 - 37$ ), the  $l$  index runs over the number of PCs and the  $k$  index runs over the number of cosmological parameters. The hyperparameters,  $\lambda_l, \rho_{kl}, \lambda_p$ , are set by exploring the likelihood surface, which is done with a Markov chain Monte Carlo analysis, but any other algorithm that locates the maximum likelihood of a multidimensional surface could also be used. The complete expression for the posterior can be found in Equation B17 of Heitmann et al. (2009). This conditions the Gaussian process to the design of the 37 models and ensures that the hyperparameters correctly capture the complexity of the surface, because they control the fit of the interpolating functions to the data.

After conditioning the GP for the best-fitting hyperparameters, the emulator is ready to predict the  $c-M$  relation for a different cosmology. The prediction involves re-calculating the covariance matrix between the new parameters and the design and this locates the new parameters within the design space. This process is quite fast, and can be repeated each time a new cosmology is needed with little computational cost.

The results at intermediate redshifts ( $0 < z < 1$ ) are produced with a simple linear interpolation. This remains fairly accurate because the change in the  $c-M$  relation with redshift is largely a simple shift in amplitude.

#### 4.2. Testing the Emulator

The accuracy of the emulator is determined using two methods: 1) we compare the performance of the emulator against a model not included in the original design and 2) we remove one of the models from the design and rebuild the emulator based on the remaining 36 models in what is known as a holdout test. In this section, we perform both of these tests to demonstrate the accuracy of the  $c-M$  emulator.

We withheld one model (M000) with a  $\Lambda$ CDM concordance cosmology from the set of 37 models when building the  $c-M$  emulator. Figure 4 shows the comparison between the emulator prediction for this cosmology against the direct simulation results from three different box sizes at  $z=0$  and  $z=1$ . The hashed region covers the 1-sigma boundary around the mean. The emulator predictions are consistent with the  $N$ -body  $c-M$  relations well within the errors on the measurements. In comparison with the smoothed fit for model M000, derived from the same power law fitting procedure used on the set of 37 cosmologies, we find that at  $z=0$ , the emulator is essentially perfect at the high mass end and accurate to at least 3.25% for low mass halos. For  $z=1$  the error is somewhat worse, mainly due to the limited halo statistics for building the emulator, especially for the low- $\sigma_8$  models. At low masses the predictions are accurate at the 2% level and degrade to 9% inaccuracy at the highest masses considered. All of these values are well within what may be considered to be the nominal uncertainty in determining concentrations from simulations (Bhattacharya et al. 2011). For most of the range of halo mass considered, the accuracy of the emulator outperforms any other prediction scheme available, especially considering the large model space covered here.

In Fig. 5, we show estimates of the emulator error by performing a holdout test. In such a test one model is kept aside and a new emulator is built, based on the remaining 36 models. The new emulator is used to predict the  $c-M$  relation for the held-out model. Since the numerical result (‘truth’) is known for that model, we can measure the emulator prediction error.

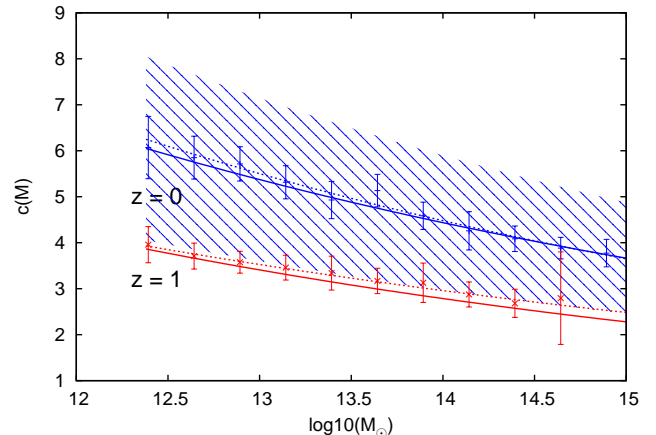


FIG. 4.— Predictions from the  $c-M$  emulator at  $z=0$  (blue, solid) and  $z=1$  (red, solid) for measurements from  $N$ -body simulations for the M000 cosmology. The dashed lines show the best-fit power law describing the  $N$ -body results and the hashed region shows the expected variation in the  $c-M$  relation from the mean (solid line). Note that this set of simulations was not used to build the emulator.

One shortcoming of this method – in particular if only a very small number of simulations is available as is the case here – is that by removing one model, the quality of the emulator is degraded. Therefore, the error estimate for the emulator obtained this way can be considered to be a conservative upper bound.

We have chosen to exclude only models M004, M008, M013, M016, M020 and M026, because these are located relatively close to the center of the design. Removing a model that defines one of the edges of the design would greatly reduce the performance of the emulator, since the GP would be extrapolating for a missing model that is now outside of the design range. The comparison is made with respect to the smoothed  $N$ -body result that was used to construct the full emulator, not the raw concentration measurements from the simulation. At most, the emulator deviates by 3.3% from the simulation results at  $z=0$  and this rises to 15% at  $z=1$ . This is because the error on the raw measurements increases with redshift as the sample size of halos decreases, particularly for low- $\sigma_8$  models.

#### 4.3. Comparison with other $c-M$ Predictions

We now compare the results obtained from the emulator with those from the models presented in Bhattacharya et al. (2011), Bullock et al. (2001), Duffy et al. (2008) and Prada et al. (2012). The Bullock et al. (2001) model was intended to correct the redshift dependence of the original NFW model, which was claimed to overpredict the concentration of high redshift ( $z > 1$ ) halos. We perform our comparisons against the most recent version of the model that incorporates corrections from Macciò et al. (2008)<sup>2</sup>. The Bullock et al. (2001) model contains two free parameters  $K = 3.85$  and  $F = 0.01$ . Newer values of  $K$  and  $F$  were obtained in Macciò et al. (2008) by fitting this model to  $N$ -body simulations using cosmological parameters corresponding to the first, third and fifth WMAP data releases. Figure 6 shows the ratio of the Bullock et al. (2001) model to our emulator at  $z=0$  for two cosmologies, M000 and WMAP7 (Komatsu et al. 2011); note that the Bullock et al. (2001) model has only been tested with  $\Lambda$ CDM and SCDM cosmologies. These two models are certainly consistent at low

<sup>2</sup> available from [physics.uci.edu/~bullock/CVIR](http://physics.uci.edu/~bullock/CVIR)

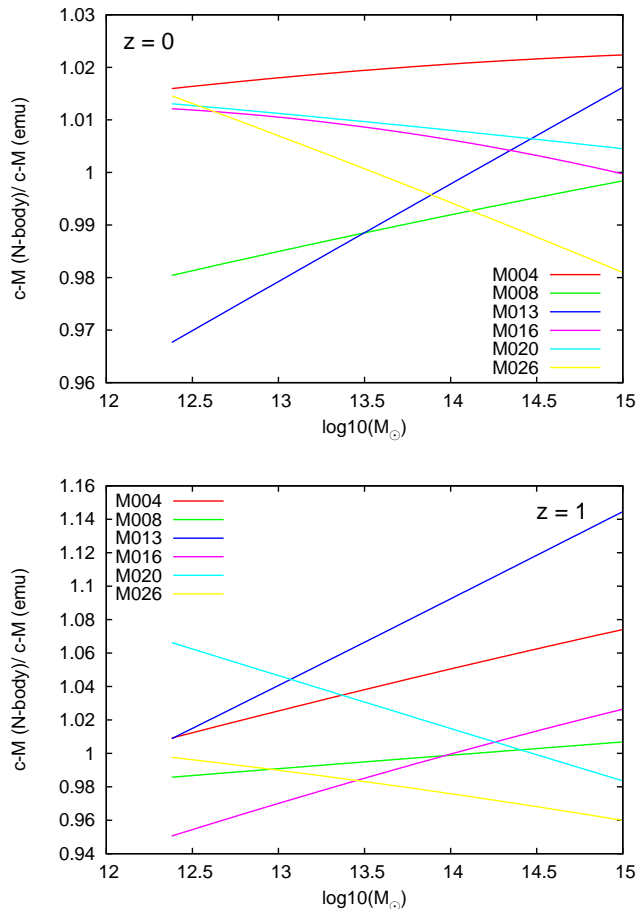


FIG. 5.— Holdout tests for the  $c-M$  emulator at  $z=0$  (top) and  $z=1$  (bottom). In both plots, the labelled model has been removed from the design and an emulator is rebuilt on the reduced design. We then take the ratio of the smoothed  $N$ -body result and the prediction from the new emulator to check the accuracy of the full emulator made with the original design.

halo masses, within the expected error of the emulator, but a substantial discrepancy occurs at cluster-sized halos, even with the updated version of Macciò et al. (2008). This occurs because the model contains free parameters that need to be tuned to a particular cosmology with  $N$ -body simulations. However, the Bullock et al. (2001) model is able to reach much lower halo masses,  $M < 10^{10} M_{\odot}$ , than our emulator because it is calibrated to higher mass resolution  $N$ -body simulations.

At  $z=1$ , the public code used for the Bullock/Macciò model fails to compute the concentration across the full range of halo masses because of difficulties at low  $\sigma_8$ . We therefore show only results for a limited mass range. The discrepancy here is much larger than for  $z=0$ , with a concentration underestimation of greater than 20%.

More recently, Duffy et al. (2008) proposed a new  $c-M$  relation with a power-law relationship between the halo mass and the concentration, as extracted from a series of high resolution, small to medium volume  $N$ -body simulations with a WMAP5 cosmology. Results from the  $c-M$  emulator are consistent with their predictions to within  $\sim 10\%$  at  $z=0$ , as are the results in Bhattacharya et al. (2011). There is a slight deviation at cluster sized halos; our  $c-M$  emulator is based on larger volume simulations, and is therefore able to provide a more complete sample of massive halos and reduced shot noise

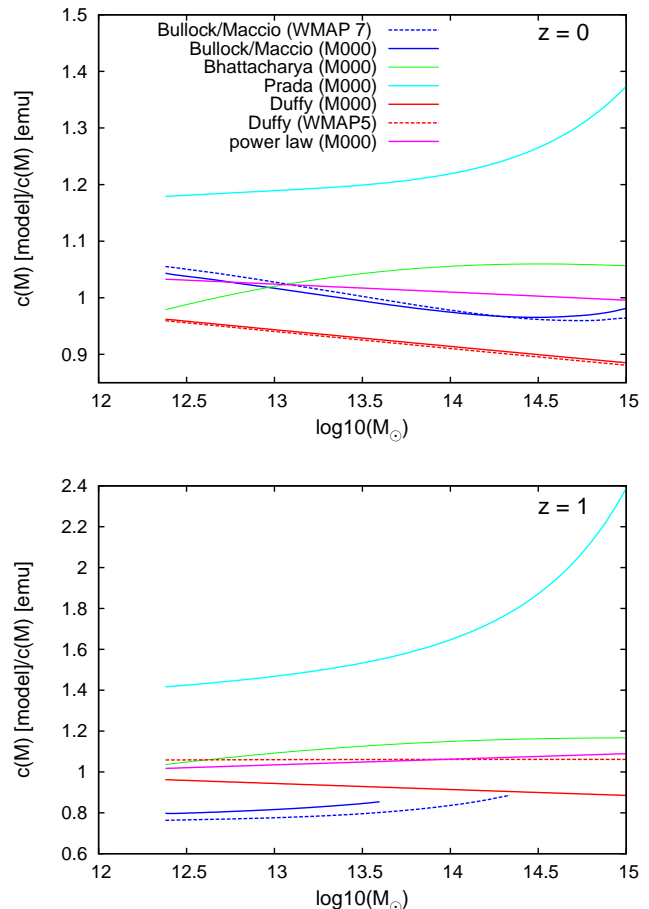


FIG. 6.— Comparison of the emulator – taken as the reference – with other models for the  $c-M$  relation at  $z=0$  (upper panel) and  $z=1$  (lower panel). The Bullock et al. (2001)/Macciò et al. (2008)  $c-M$  relation is shown in blue for both M000 (solid) and WMAP7 (dashed) cosmologies. The Bhattacharya et al. (2011) fit (note that this fit was derived only for M000, not for general cosmological models) is in green, the Prada et al. (2012)  $c-M$  relation in cyan, and the Duffy et al. (2008)  $c-M$  relation in red for M000 (solid) and WMAP5 (dashed) cosmologies. In addition, the pink line shows the ratio of the power-law fit for M000 to the emulator prediction (As shown in Fig. 4 the agreement is very good, with less than 3% deviation over most of the mass range). The lower panel shows the results for  $z=1$ . The publicly available code for the Bullock et al. (2001)/Macciò et al. (2008) fit does not work seamlessly over the full mass range so we do not show results for the very high mass end here. See the text for further discussion of this set of results.

at the high mass end. The agreement between the emulator and the Duffy et al. (2008)  $c-M$  relation improves to  $\sim 5-6\%$  at  $z=1$  for the WMAP5 cosmology.

In Figure 6, we also show the ratio between our emulator and the  $c-M$  relation as determined by the model discussed in Prada et al. (2012), which is itself based on a number of  $N$ -body simulations. There is a  $\sim 20\%$  discrepancy at  $z=0$  ( $\sim 40\%$  at  $z=1$ ) for lower halo masses. This increases dramatically for cluster sized haloes at both redshifts, since unlike Prada et al. (2012), we do not observe an upturn in the  $c-M$  relation, where their concentration increases with halo mass. One should note that the methods for measuring the halo concentration are different in our two cases – we use a finite-range profile-fitting method as discussed in Bhattacharya et al. (2011), whereas Prada et al. (2012) use a two-point ratio method.

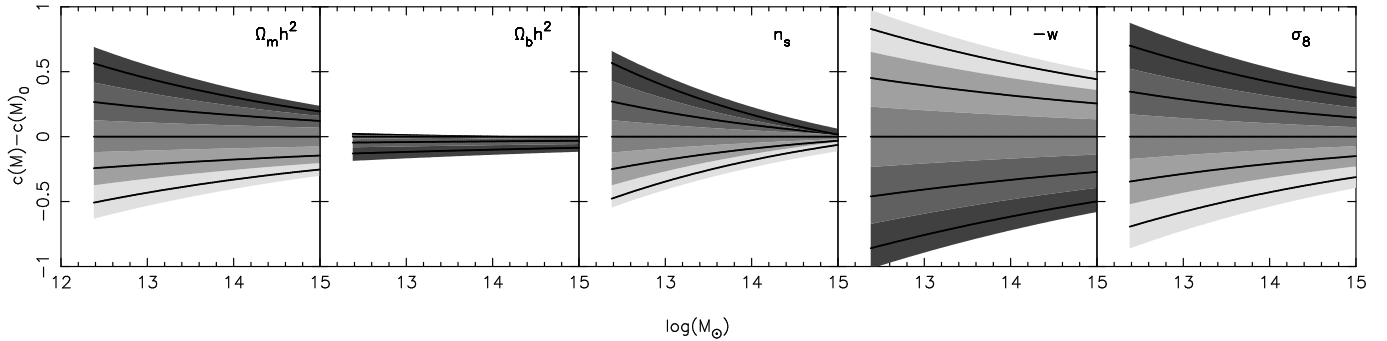


FIG. 7.— Sensitivity of the  $c-M$  relation to the five cosmological parameters varied in the emulator design,  $\Omega_m h^2$ ,  $\Omega_b h^2$ ,  $-w$ ,  $n_s$  and  $\sigma_8$ , at  $z=0$ . We vary each cosmological parameter individually for each panel and have binned the range into five intervals, which are coloured from light to dark as the value of the parameter increases. From each of these, we subtract the  $c-M$  relation for the model corresponding to the midpoint of the design space,  $c(M)_0$ . To guide the eye, we also plot the median  $c(M) - c(M)_0$  of each bin in parameter space.

Expectations for discrepancies between profile fitting and their particular ratio method are further discussed in the appendix of Bhattacharya et al. (2011).

We also note that there is a good agreement to within  $\sim 5\%$  between our emulator and the  $c-M$  relations measured by Neto et al. (2007) from the Millennium simulation Springel (2005b). The cosmology of the Millennium simulation does not quite fall within the range of our emulator ( $\omega_b h^2 = 0.024$  and  $h = 0.73$ ), and to facilitate this comparison, we have adopted values as close to these as possible that still lie within our parameter space ( $\omega_b h^2 = 0.0235$  and  $h = 0.719$ ).

Lastly, we compare the emulator prediction with the fitting function derived in Bhattacharya et al. (2011) for the M000 cosmology. Before doing so, we provide some necessary background. First, the redshift dependence in the fitting form in Bhattacharya et al. (2011) is handled differently than in the current paper. In Bhattacharya et al. (2011), the aim was to find a global power-law fit that encompasses all redshifts considered (between  $z=0$  and  $z=2$ ) at once. Therefore, the fit for each redshift is not expected to be perfect. In the current paper we follow a different path: since we do not provide a single formula for the  $c-M$  relation but rather a simple numerical code, we can generate the best-fit power-law model for each redshift separately and then simply interpolate between the redshifts. This produces a more accurate answer at each redshift at the minimal cost of running a fast code for every  $c-M$  prediction instead of using one fitting formula.

Second, for the high-mass range, Bhattacharya et al. (2011) used higher force resolution simulations. As shown in the Appendix of Bhattacharya et al. (2011), the concentrations from the Coyote runs are slightly lower at high masses (at the 5% level) compared to higher-resolution simulations. Since it is not clear if this effect is independent of cosmology (most likely for lower  $\sigma_8$  simulations the effect will be smaller) we decided to not attempt to correct the concentration measures in this paper for the Coyote runs. Therefore, the uncertainty for the high mass concentrations from the emulator predictions will be slightly higher and one expects the predictions to be biased slightly low. Considering the overall scatter and uncertainty in the  $c-M$  relation, this small effect is unlikely to be significant. One should note, however, that due to this suppression, the ratio of  $\sigma_c(M)$  to the mean concentration, which we quote at the nominal value of  $1/3$ , could be slightly smaller at higher masses.

Keeping these caveats in mind, we now turn to the comparison of the fit by Bhattacharya et al. (2011) and the emulator

result, in Fig. 6. For  $z=0$ , both agree at the 2% (low halo mass) to 6% (high halo mass) level, the Bhattacharya et al. (2011) fit being slightly higher as expected. For  $z=1$ , the discrepancy ranges from 4% to 17%. Here, overall the emulator estimate compared to the best-fit power-law to the simulation result is slightly low, while the Bhattacharya et al. (2011) fit slightly overestimates the simulation results. In other words, the actual simulation result lies in between the emulator prediction and the fit. Overall, the agreement between the Bhattacharya et al. (2011) fit and the emulator is much better at  $z=1$  than the agreement between the emulator and the Bullock/Macció fit.

#### 4.4. Cosmology Dependence of the $c-M$ Relation

Finally, we explore the sensitivity of the  $c-M$  relation to variations in cosmology. Since we now have a means of quickly and smoothly interpolating from one cosmology to another, we can simply vary the parameters that we incorporated into our design space in a regular grid. We divide each parameter range into five evenly spaced regions and vary only a single parameter at a time by keeping the other four parameters fixed at the midpoint of the parameter range. Our comparisons are always made with respect to this model at the midpoint, which has the parameters:  $\Omega_m h^2 = 0.1375$ ,  $\Omega_b h^2 = 0.0225$ ,  $n_s = 0.95$ ,  $w = -1$  and  $\sigma_8 = 0.758$ , and is subtracted from each  $c-M$  relation. Figure 7 shows the results of this exercise at  $z=0$ , with the values of the cosmological parameters increasing as the shading increases from light to dark. The entire region is coloured to show the variation in the  $c-M$  relation across each parameter bin. The range of concentration variation changes as a function of mass and the cosmological parameter being varied; the largest variation is of order unity. Unsurprisingly, the  $c-M$  relation increases with  $\Omega_m h^2$  and  $\sigma_8$  and decreases with  $w$ , which slows the rate of structure formation. We see little variation with  $\Omega_b h^2$  because the range of parameters allowed by the CMB constraints is already quite tight. Also, cluster-sized halos appear to be relatively less sensitive to these changes in cosmology. Figure 7 also shows a clear degeneracy between  $\Omega_m h^2$ ,  $\sigma_8$ , and  $n_s$  in the  $c-M$  relation.

## 5. CONCLUSION AND OUTLOOK

In this paper, we have presented a new prediction scheme – in the form of an emulator – for the  $c-M$  relation for dark matter-dominated halos at the bright galaxy to cluster mass scales, covering a range of  $2 \cdot 10^{12} M_\odot < M < 10^{15} M_\odot$  and a redshift range of  $z=0$  to  $z=1$ . The emulator provides results for a large class



of  $w$ CDM cosmologies and is accurate at the  $\sim 5\%$  level (better for lower redshifts, slightly worse for higher redshifts). The emulator enables consistent predictions to be made when testing for deviations from  $\Lambda$ CDM using clusters. This is particularly important for cluster cosmology, since the behaviour of the  $c-M$  relation can vary by as much as 30% just by varying the equation of state across the range  $-1.3 < w < -0.7$ . By correctly including the cosmology dependence in the  $c-M$  relation, the emulator improves on analytic modelling of halo profiles, such as the 1-halo term used in the halo power spectrum. The performance of the emulator compares favourably with the other models for the  $c-M$  relation in the literature and outperforms the Bullock/Macció model across the redshift and mass range considered.

Aside from predicting the mean  $c-M$  relation, the interesting and useful fact that across all 37 cosmologies considered, 1) the scatter in halo concentrations in individual mass bins is Gaussian, and 2) the corresponding standard deviation is given by roughly a third of the mean concentration value, means that the  $c-M$  emulator also includes within it the information regarding the concentration distribution at a given value of mass.

The work in this paper is an example of how the cosmic calibration framework provides a means of estimating highly nonlinear quantities involving evolved structures from a limited number of computationally expensive  $N$ -body simulations. In the future, we will extend the number and range of cosmological parameters to include more exotic phenomena, such as evolving dark energy, as a complement to upcoming dark energy experiments.

The work at Argonne National Laboratory was supported under U.S. Department of Energy contract DE-AC02-06CH11357. Part of this research was supported by the DOE under contract W-7405-ENG-36. We are indebted to Charlie Nakhleh for providing an example code for building cosmic emulators and Earl Lawrence and Dave Higdon for many useful and entertaining discussions on the topic. We thank Volker Springel for making GADGET-2 publicly available. We are grateful for computing time granted to us as part of the Los Alamos Open Supercomputing Initiative. This research used resources of the Argonne Leadership Computing Facility at Argonne National Laboratory and the National Energy Research Scientific Computing Center, which are supported by the Office of Science of the U.S. Department of Energy under contract DE-AC02-06CH11357 and DE-AC02-05CH11231 respectively.

## REFERENCES

- Bhattacharya, S., Heitmann, K., White, M., Lukić, Z., Wagner, C., & Habib, S. 2011, *ApJ*, 732, 211
- Bhattacharya, S., Habib, S., Heitmann, K., & Vikhlinin, A. 2011, arXiv:1112.5479
- Bullock, J., Kolatt, T.S., Sigad, Y., Somerville, R.S., Kravtsov, A.V., Klypin, A.A., Primack, J.R., & Dekel, A. 2001, *MNRAS*, 321, 559
- Duffy, A.R., Schaye, J., Kay, S.T., & Dalla Vecchia, C. 2008, *MNRAS*, 390, L64
- Duffy, A.R., Schaye, J., Kay, S.T., Dalla Vecchia, C., Batty, R.A., & Booth, C.M. 2010, *MNRAS*, 405, 2161
- Eifler, T. arXiv:1012.2978
- Eke, V.R., Navarro, J.F., & Steinmetz, M. 2001, *ApJ*, 554, 114
- Gao, L., Navarro, J.F., Cole, S., Frenk, C.S., White, S.D.M., Springel, V., Jenkins, A., & Neto, A.F. 2008, *MNRAS*, 387, 536
- Habib, S., Heitmann, K., Higdon, D., Nakhleh, C., & Williams, B. 2007, *Phys. Rev. D* 76, 083503
- Habib, S., Pope, A., Lukić, Z., Daniel, D., Fasel, P., Desai, N., Heitmann, K., Hsu, C.-H., Ankeny, L., Mark G., Bhattacharya, S., & Ahrens, J., 2009, *Journal of Physics: Conference Series*, 180, 012019
- Hayashi, E. & White, S.D.M. 2008, *MNRAS*, 388, 2
- Heitmann, K., Higdon, D., Nakhleh, C., & Habib, S. 2006, *ApJ* 646, L1
- Heitmann K., Higdon D., White M., Habib S., Williams, B.J., & Wagner, C. 2009, *Astrophys. J.* 705, 156
- Heitmann K., White M., Wagner C., Habib S., & Higdon D. 2010 *Astrophys. J.* 715, 104
- Komatsu, E. et al., 2011, *ApJS*, 192, 18
- Lawrence, E., Heitmann, K., White M., Higdon D., Wagner C., Habib S., & Williams, B. 2010, *ApJ*, 713, 1322
- Li, W. & Ye, K.Q. 2000, *Journal of Statistical Planning and Inference*, 90, 145
- Lukić, Z., Reed, D., Habib, S., & Heitmann, K. 2009, *ApJ*, 692, 217
- Macció, A., Dutton, A., & van den Bosch, F.C. 2008, *MNRAS*, 291, 1940
- More, S., Kravtsov, A.V., Dalal, N., & Gottlöber, S. 2011, *ApJS*, 195, 4
- Navarro, J.F., Frenk, C.S., & White, S.D.M. 1996, *ApJ*, 462, 563
- Navarro, J.F., Frenk, C.S., & White, S.D.M. 1997, *ApJ*, 490, 493
- Neto, A. F., Gao, L., Bett, P., Cole, S., Navarro, J. F., Frenk, C. S., White, S. D. M., Springel, V. & Jenkins, A., 2007, *MNRAS*, 381, 1450
- Oguri, M., Bayliss, M.B., Dahle, H., Sharon, K., Gladders, M.D., Natarajan, P., Hennawi, J.F., & Koester, B.P. 2011, arXiv:1109.2594v2 [astro-ph.CO]
- Pope, A., Habib, S., Lukić, Z., Daniel, D., Fasel, P., Desai, N., & Heitmann, K. 2010, *Comp. Sci. & Eng.* 12, 17
- Prada, F., Klypin, A.A., Cuesta, A.J., Betancort-Rijo, J.E., & Primack, J. 2012 *MNRAS*, 423, 3018
- Santner, T.J., Williams, B.J., & Notz, W.I. 2003, *The Design and Analysis of Computer Experiments*, Springer, New York
- Schneider, M., Knox, L., Habib, S., Heitmann, K., Higdon, D., & Nakhleh, C. 2008, *Phys. Rev. D*, 78, 063529
- Springel, V. 2005, *MNRAS*, 364, 1105
- Springel, V., White, S. D. M., Jenkins, A., Frenk, C. S., Yoshida, N., Gao, L., Navarro, J., & Thacker, R. et al., 2005, *Nature*, 435, 629
- Vikhlinin, A., Kravtsov, A.V., Burenin, R.A., Ebeling, H., Forman, W.R., Hornstrup, A., Jones, C., Murray, S.S., Nagai, D., Quintana, H., & Voevodkin, A. 2009, *ApJ*, 692, 1060
- White, M. 2011, *A&A* 367, 27
- Woodring, J., Heitmann, K., Ahrens, J., Fasel, P., Hsu, C.H., Habib, S., & Pope, A. 2011, *ApJS*, 195, 11
- Wu, H.-Y., Hahn, O., Wechsler, R.H., Mao, Y.-Y., & Behroozi, P.S. arXiv:1209.3309 [astro-ph.CO]
- Zhao, D.H., Jing, Y.P., Mo, H.J., & Börner, G. 2009, *ApJ*, 707, 354